Journal of Physics and Chemistry of Solids 75 (2014) 334–338

Contents lists available at ScienceDirect

Journal of Physics and Chemistry of Solids

journal homepage: www.elsevier.com/locate/jpcs

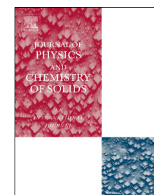

Nanotribological behavior of ZnO films prepared by atomic layer deposition

Wun-Kai Wang [a,1], Hua-Chiang Wen [b,1], Chun-Hu Cheng [c], Wu-Ching Chou [b], Wei-Hung Yau [d,*], Ching-Hua Hung [a], Chang-Pin Chou [a]

[a] Department of Mechanical Engineering, National Chiao Tung University, Hsinchu 300, Taiwan, ROC
[b] Department of Electrophysics, National Chiao Tung University, Hsinchu 300, Taiwan, ROC
[c] Department of Mechantronic Technology, National Normal University, Taipei 106, Taiwan, ROC
[d] Department of Mechanical Engineering, Chin-Yi University of Technology, Taichung 400, Taiwan, ROC

A R T I C L E I N F O

Article history:
Received 20 February 2013
Received in revised form
14 August 2013
Accepted 18 September 2013
Available online 12 October 2013

Keywords:
A. Thin films
B. Vapor deposition
C. Mechanical properties

A B S T R A C T

We used atomic layer deposition to form ZnO thin-film coatings on Si substrates and then evaluate the effect of pile-up using the nanoscratch technique under a ramped mode. The wear volume decreased with increasing annealing temperature from room temperature to 400 °C for a given load. Elastic-to-plastic deformation occurred during sliding scratch processing between the groove and film for loading penetration of 30 nm. The onset of non-elastic behavior and greater contact pressure were evident for loading penetration of 150 nm; thus, full plastic deformation occurred as a result of a substrate effect. We suspect that elastic–plastic failure events were related to edge bulging between the groove and film, with elastic–plastic deformation attributable to adhesion discontinuities and/or cohesion failure of the ZnO films.

© 2013 Elsevier Ltd. All rights reserved.

1. Introduction

Zinc oxide (ZnO), a metal oxide that form transparent films, is a wide-bandgap semiconductor with high thermal and chemical stability and large exciton binding energy (∼60 meV); it is one of the main materials used in blue and UV optical devices [1–3]. ZnO can be deposited as a thin film using several techniques, including pulsed laser deposition, spray pyrolysis, and aqueous solution methods [4–6]. In recent years, atomic layer deposition (ALD) has become an attractive method for the formation of smooth films, with the additional benefits of high conformality and precise control over thickness and composition. ALD formation of ZnO through cyclic self-limiting deposition can yield conformal and uniform thin films at the atomic level [7,8]. The electrical, optical, and structural properties of such ZnO materials have been investigated in detail for various processing parameters and conditions [9].

ZnO films have recently been used in acoustic wave biosensing and microfluidic applications; their potential utility in the fabrication of lap-on-chip (LOC) systems may affect the development of the biotechnology industry. Kim et al. reported that a passivated ALD aluminum oxide surface could be used in an acoustic wave sensor for early biofilm detection [10]. Most acoustic wave devices need to be sensitive to input signals, such as mechanical stress, chemical exchange, and electrical perturbations. Thus, a strong texture, a low density of defect traps, a smooth surface, and good stoichiometry are basic requirements for good piezoelectric properties. As mentioned above, ALD with precise compositional control using layer-by-layer deposition can meet these requirements at a low thermal budget of 200 °C; the ability to integrate ALD with CMOS processing is useful in the preparation of LOC systems. However, the acoustic velocity of a ZnO film strongly depends on substrate effects due to lattice mismatch, which limits the piezoelectric properties. The crystallinity of a ZnO film is responsible for its piezoelectric response. Although the crystallinity can be improved via high-temperature annealing, the interface quality will suffer from adhesion issues as a result of local strain or stress originating from de-bonding of Zn atoms [11].

Nanoindentation can provide a good understanding of the mechanical properties of a thin film interface, primarily its elastic–plastic properties, friction, and adhesion. These parameters characterize the mechanical stability of a working device and can provide useful predictions regarding durability. Nanoindentation is performed using an instrument that measures force and displacement continuously during indentation [13–18]. Slip band movement and dislocation nucleation mechanisms have been proposed to explain pop-in events within the epilayers of ZnO films [14–17].

* Corresponding author. Tel.: +886 423924505; fax: +886 423930681.
E-mail address: ywhung1@gmail.com (W.-H. Yau).
[1] These authors contributed equally to this work.

0022-3697/$ - see front matter © 2013 Elsevier Ltd. All rights reserved.
http://dx.doi.org/10.1016/j.jpcs.2013.09.016

Annealing treatment is commonly applied to minimize defects and improve the quality of as-grown thin films. Kim et al. found that annealing significantly improved the optical properties and surface morphology of ALD ZnO thin films compared to as-grown samples [12].

In this study we investigated the nanotribological behavior of ALD ZnO films and the temperature-dependent crystallization effects of different annealing conditions. To gain an insight into the failure mechanisms involved in nanotribological responses, we analyzed the surface morphology, film crystallinity, microstructure, and adhesion and cohesion using atomic force microscopy (AFM), X-ray diffraction (XRD), transmission electron microscopy (TEM), and scanning probe microscopy (SPM). We also examined the quality of the resulting ZnO layers in terms of pile-up events under sliding scratch-induced deformation.

2. Experimental

Water and diethylzinc were used as precursors and nitrogen as the purge gas. Thin ZnO films were deposited on Si (1 0 0) substrates at 200 °C in an ALD system operated using the flow-rate interruption method [8,19]. The number of deposition cycles was fixed at 150 in each experiment and the deposition rate was controlled at 0.2 Å per cycle. The thickness of each as-deposited ZnO film was approximately 30 nm. As-deposited ZnO films were subjected to rapid thermal annealing at 300 or 400 °C for 1 h under N_2. The heating rate was set at 20 °C s^{-1}; the furnace required approximately 30 min to cool to RT after annealing. The ZnO crystallinity was analyzed using XRD (PANalytical X'Pert Pro, MRD) with Cu K_α (λ=0.154 nm) radiation. Scans were conducted over the 2θ range 20–80° (scan rate 2° min^{-1}) at a grazing angle of 0.5° under 30 kV and 30 mA. XRD data conformed to the Joint Committee on Powder Diffraction Standards card (JPCDS). Cross-sectional TEM (JEOL JEM-2010F, operating voltage 200 kV) was used to examine the ZnO/Si microstructure.

The nanotribological properties of ZnO films were determined using an SPM system in which AFM (Digital Instruments Nanoscope III) was combined with a nanoscratch measurement system. The scanning probe microscope (Hysitron Corporation) was operated at a constant scan rate of 2 μm s^{-1}. The adhesion properties of as-deposited samples and samples annealed at 300 and 400 °C were evaluated using a nanoindentation system. The constant depth mode was used and penetration depths of 30 and 150 nm were applied for each ZnO film. The maximum load was maintained while forming 10-μm-long scratches. Surface profiles before and after scratching were obtained by scanning the tip at a normal load of 0.02 mN (i.e., a load sufficiently small to produce any measurable displacement). After scratching, the wear tracks were imaged using AFM.

3. Results and discussion

Fig. 1 shows XRD patterns for as-deposited ZnO and samples annealed at 300 and 400 °C. The diffraction peaks for ZnO (1 0 0), (0 0 2), (1 0 1), (1 0 2), (1 1 0), (1 0 3), and (1 1 2) evident in the XRD patterns confirm that all the films were polycrystalline with a hexagonal wurtzite structure. The intensity of the ZnO (0 0 2) peak was higher for the sample annealed at 400 °C than for the film annealed at 300 °C, indicating that the higher annealing temperature increased the crystallinity. The results suggest that the ZnO layer remained largely polycrystalline with excellent crystalline quality.

We obtained more detailed structural information using TEM. Fig. 2 shows a cross-sectional TEM image of the ZnO/Si system,

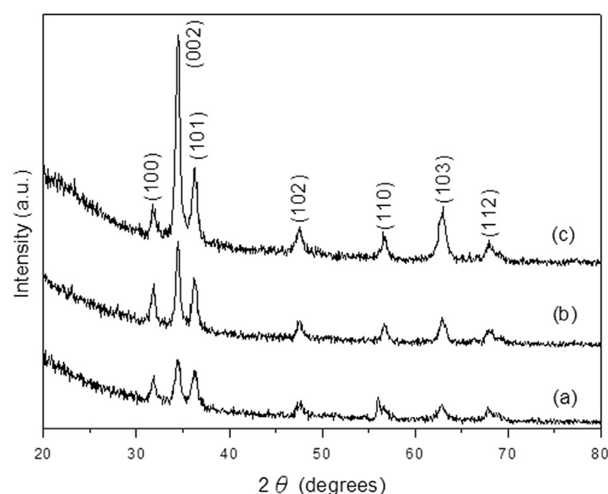

Fig. 1. XRD patterns for ALD ZnO films. (a) As-deposited film and films annealed at (b) 300 °C and (c) 400 °C.

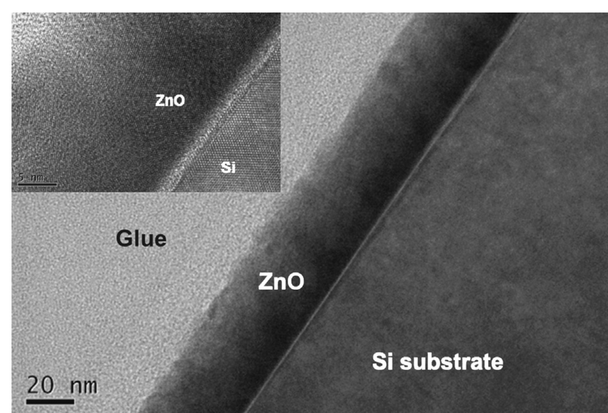

Fig. 2. Cross-sectional TEM image of the ZnO/Si system.

which features a layer of polycrystalline ZnO. Randomly oriented ZnO nanocrystals within the 30-nm-thick ZnO layers appear to have very good crystallinity. A nanometer-thick interface region is evident between Si and the ZnO layer. This interface appears blurred and the ZnO grains it contains have relatively poor crystallinity. As described below, this interface has a significant effect on the ZnO/Si adhesion properties.

Fig. 3 presents typical AFM profiles of ZnO films deposited on Si before and after nanoscratch tests at a penetration of 30 or 150 nm. The scratch images reveal that an increase in load led to an increase in wear volume (total volume swiped by the indenter tip) for each ZnO coating; the wear volume is consistent with the projected area of the indenter tip. Using such a scratch system to determine elastic–plastic contact, Pelletier et al. found that the shape of the residual groove was related to the plastic strain field [20]. The profile in Fig. 3a indicates that the surface material underwent an elastic reaction as a result of elastic deformation between the groove and the film when the penetration depth was 30 nm. The indenter resulted in greater contact pressure for the sample annealed at 300 °C, leading to the onset of non-elastic behavior (Fig. 3b). For the sample annealed at 400 °C, large areas of the coating were removed from the scratch track as a result of elastic–plastic deformation at 30 nm (Fig. 3c). The penetration depth traces reveal a slight increase for the sample treated at 400 °C compared to the sample treated at 300 °C. This SPM trend matches the lateral force curves in Fig. 4a, from which it is evident that an elastic reaction between the groove and film dominates. A similar response is evident in Fig. 3d–f: an increase in lateral

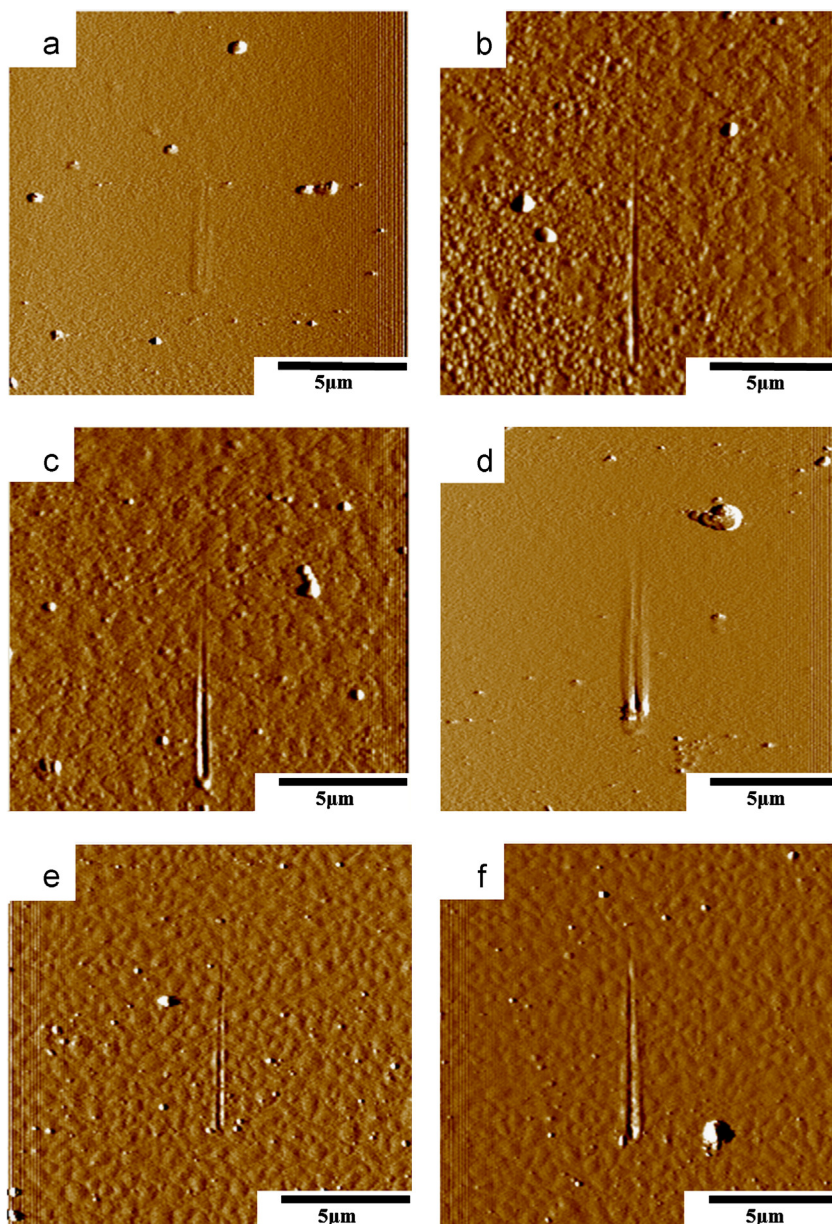

Fig. 3. AFM images combined with nanoscratch trace measurements for nanoscratched samples obtained using a ramp force at a depth of (a–c) 30 nm and (d–f) 150 nm. (a,d) As-deposited sample; (b,e) sample annealed at 300 °C; and (c,f) sample annealed at 400 °C.

force is evident for a penetration depth of 150 nm, without marked oscillations. However, the substrate effect may dominate as a result of the increased lateral force.

The annealing temperature was sufficient to drive transformation to a denser crystal structure so that ductile deformation was inhibited. The critical load was 29.8 and 50.6 μN for the samples annealed at 300 and 400 °C, respectively. No signal was detected for the as-deposited sample. Sample annealing at 400 °C led to relaxed crystallization of the ZnO coating, as observed in Fig. 4a,b. The changes in scratch groove morphology also indicate an improvement in the nanoscale wear resistance. At the beginning of each scan, all of the films exhibited similar behavior, but the effect of the annealing temperature became apparent thereafter. This behavior may be due in part to shrinkage events, attributable to a very thin coating that responds to a susceptible defect density for scratch tests at a penetration depth of 30 nm. Schreiber and Vasnyov used dynamic-mode cathodoluminescence to observe local plastic deformation during *in situ* scratching of a (0001) ZnO sample [22]. They found evidence of the propagation of highly mobile dislocations in various prismatic slip systems for their as-deposited samples. Thus, we suspect that the features of the nanoscratch zone in the vicinity of the interface might not be merely accidental artifacts resulting from sample preparation [18]. Additional evidence will be required because this phenomenon controls oscillations under friction, thereby affecting the adhesion and/or cohesion failure of ZnO films. Fig. 5a shows the friction coefficient recorded at a penetration depth of 30 nm. Oscillations under the friction force are evident, particularly for an annealing temperature of 400 °C. Owing to thin film elastic deformation, the friction coefficient decreased, gradually approaching the true value; elastic–plastic deformation of the friction coefficient was slightly disrupted in the interval 15–25 s. At 22.5 s, film dislocation caused oscillation of the friction coefficient, which then stabilized at 25 s. The friction coefficient recorded at a penetration depth of 150 nm (Fig. 5b) also exhibited oscillation under the friction force. Similar analysis of scratched films has been reported previously [19,20]. Notably, oscillation trends for each sample were similar in both on- and off-load scans [21]. The oscillations in the plots

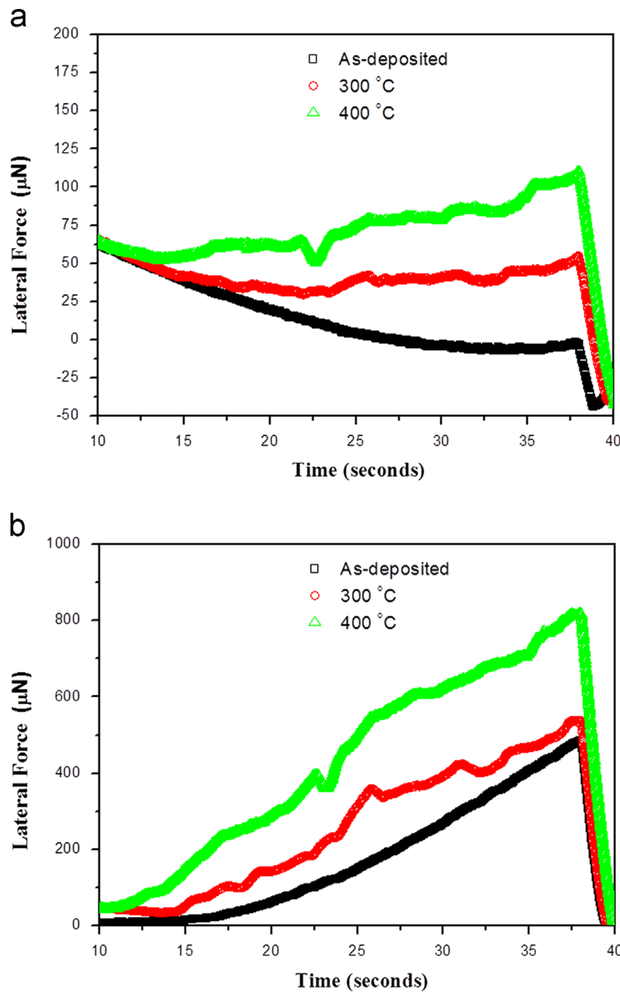

Fig. 4. Normal displacement plotted with respect to scratch duration for ZnO films annealed at 300 and 400 °C. Each sample was subjected to penetration at (a) 30 nm and (b) 150 nm.

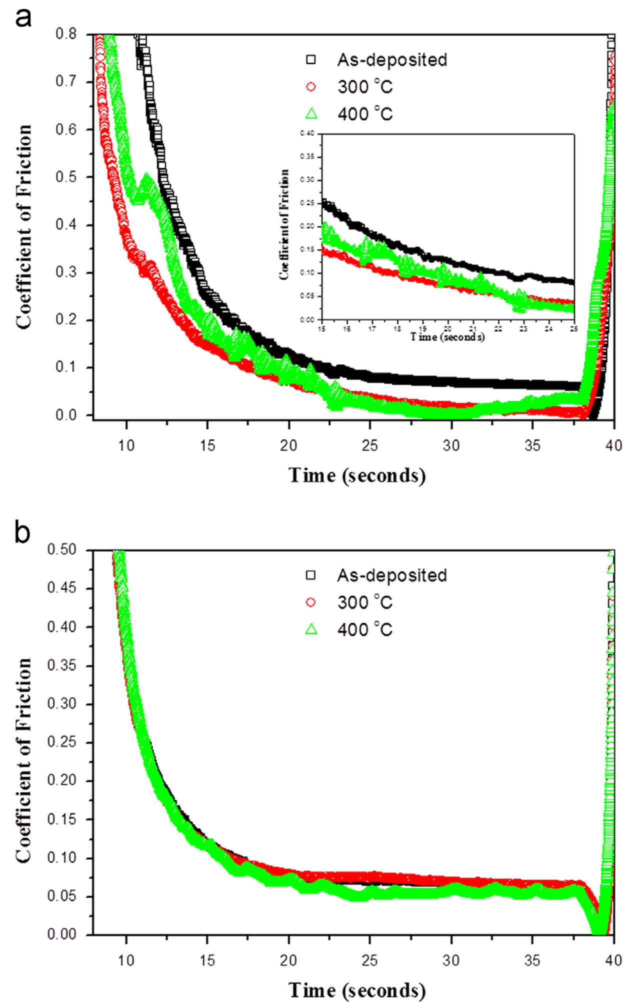

Fig. 5. Coefficient of friction (μ) plotted with respect to scratch duration for as-deposited ZnO film and films annealed at 300 and 400 °C for penetration depths of (a) 30 nm and (b) 150 nm. Inset to (a): 15–25-s interval.

recorded at a penetration depth of 150 nm are more stable than those recorded at 30 nm. We suspect that the lower degree of adhesion reflects interlinks and rearrangements that tend to result in fluctuations of the friction coefficient (μ) at a penetration depth of 150 nm. Instability in the initial μ profile, so-called pile-up, is evident in Fig. 5a for the sample annealed at 300 °C. We calculated values of μ for the ZnO films by averaging results measured at scratch durations ranging from 8 to 38 s (Fig. 6). From the trends observed in our nanotribological investigations, changes in the value of μ appear to signal the onset of adhesive failure, with cracking or delamination resulting between the interface and the sliding nanoscratch track [15,23].

The discordant curves and irregularities observed during elastic and plastic deformation can be attributed to adhesion discontinuities and/or cohesion failure, as determined from the nanoscratch traces (induction of pile-up) [24,25]. The profile for the sample annealed at 400 °C was softer than for the as-deposited sample owing to shrinkage of the nanoscratch traces. Thus, the ZnO film structure changed when the thermal treatment temperature was increased from 300 to 400 °C, presumably via alteration of the composition of the intrinsic structure. Hence, edge bulging occurred between the groove and film and the material was crushed as a result of elastic failure. In summary, the friction traces were fairly reproducible, but varied greatly for the different samples.

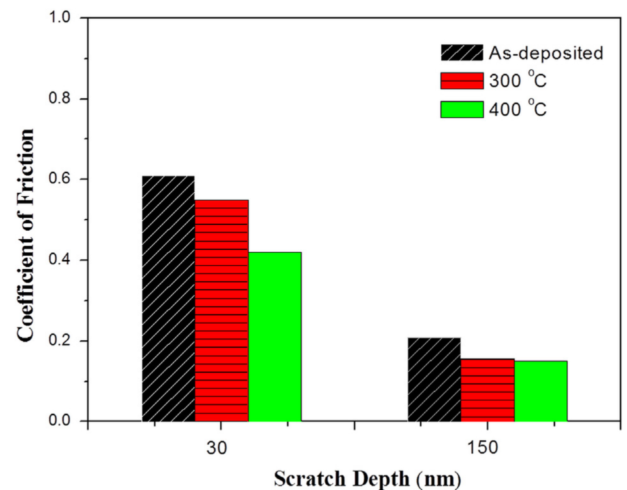

Fig. 6. Distinct critical coefficient of friction for ZnO films annealed at various temperatures and then subjected to penetration at depths of 30 and 150 nm.

4. Conclusion

We used AFM and nanoscratch techniques to characterize high-quality ALD ZnO films on Si substrates. We performed nanoscratch tests to determine the adhesion/cohesion failure mechanism of

ZnO-coated Si. An increase in annealing temperature was sufficient to drive transformation to a denser crystal structure so that ductile deformation was inhibited. Pile-up occurred at a penetration force of 29.8 and 50.6 μN for samples annealed at 300 and 400 °C, respectively. The systems exhibited significant suppression of lateral indented deformation, which induced a degree of pile-up. In addition, tip drop and lift phenomena can be explained in terms of film stiffness as a function of interatomic distances during scratch tests. For ZnO films compressed by an indenter, more μ oscillations were observed for a penetration depth of 30 nm than for 150 nm. It is reasonable to suspect that edge bulging occurred between the groove and film, resulting in elastic failure.

Acknowledgment

This study was supported by the National Science Council of Taiwan (grant nos. NSC 101–2221-E-167-004 and NSC 102–2221-E-167-007) and the National Chin-Yi University of Technology (NCUT11-REM-004: 2012.1.1–2012.10.31 and NCUT 12-REM-003: 2013.1.1–2013.10.31). We thank Dr. H.C. Wen and Prof. W.C. Chou for technical suggestions, and Prof. Y.R. Jeng for the SPM equipment used in this study.

References

[1] A.P. Alivisatos, Science 271 (1996) 933–937.
[2] K.C. Aw, Z. Tsakadze, A. Lohani, S. Mhaisalkar, Scr. Mater 60 (2009) 48–51.
[3] Y.R. Ryu, T.S. Lee, J.A. Lubguban, H.W. White, B.J. Kim, Y.S. Park, C.J. Youn, Appl. Phys. Lett. 88 (2006) 241108.
[4] S. Christoulakis, M. Suchea, E. Koudoumas, M. Katharakis, N. Katsarakis, G. Kiriakidis, Appl. Surf. Sci. 252 (2006) 5351–5354.
[5] I. Kortidis, K. Moschovis, F.A. Mahmoud, G. Kiriakidis, Thin Solid Films 518 (2009) 1208–1213.
[6] X.X. Liu, Z.G. Jin, S.J. Bu, J. Zhao, Z.F. Liu, J. Am. Ceram. Soc. 89 (2006) 1226–1231.
[7] Y.H. Lin, Y.C. Lai, C.L. Lu, W.K. Hsu, J. Mater. Chem. 21 (2011) 12485–12488.
[8] H.C. Wen, C.I. Hung, H.J. Tsai, C.K. Lu, Y.C. Lai, W.K. Hsu, J. Mater. Chem. 22 (2012) 13747–13750.
[9] Y.W. Zhu, H.I. Elim, Y.L. Foo, T. Yu, Y.J. Liu, W. Ji, J.Y. Lee, Z.X. Shen, A.T.S. Wee, J.T.L. Thong, C.H. Sow, Adv. Mater. 18 (2006) 587–592.
[10] Y.W. Kim, S.E. Sardari, M.T. Meyer, A.A. Iliadis, H.C. Wu, W.E. Bentley, R. Ghodssi, Sens. Actuators B 163 (2012) 136–145.
[11] T. Riemann, J. Christen, G. Kaczmarczyk, A. Kaschner, A. Hoffmann, A. Zeuner, D. Hofmann, B.K. Meyer, Phys. Status Solidi b 229 (2002) 891–895.
[12] C.R. Kim, C.M. Shin, J.Y. Lee, J.H. Heo, T.M. Lee, J.H. Park, H. Ryu, C.S. Son, J.H. Chang, Curr. Appl. Phys. 10 (2010) S294–S297.
[13] C.Y. Yen, S.R. Jian, G.J. Chen, C.M. Lin, H.Y. Lee, W.C. Ke, Y.Y. Liao, P.F. Yang, C.T. Wang, Y.S. Lai, J.S.C. Jang, J.Y. Juang, Appl. Surf. Sci. 257 (2011) 7900–7905.
[14] W.H. Yau, P.C. Tseng, H.C. Wen, C.H. Tsai, W.C. Chou, Microelectron. Reliab. 51 (2011) 931–935.
[15] M.H. Lin, H.C. Wen, Y.R. Jeng, C.P. Chou, Nanoscale Res. Lett. 5 (2010) 1812–1816.
[16] M.H. Lin, H.C. Wen, C.Y. Huang, Y.R. Jeng, W.H. Yau, W.F. Wu, C.P. Chou, Appl. Surf. Sci. 256 (2010) 3464–3467.
[17] H.C. Wen, C.S. Yang, W.C. Chou, Appl. Surf. Sci. 256 (2010) 2128–2131.
[18] S.R. Jian, I.J. Teng, P.F. Yang, Y.S. Lai, J.M. Lu, J.G. Chang, S.P. Ju, Nanoscale Res. Lett. 3 (2008) 186–193.
[19] C.J. Hu, Y.H. Lin, C.W. Tang, M.Y. Tsai, W.K. Hsu, H.F. Kuo, Adv. Mater. 23 (2011) 2941–2945.
[20] H. Pelletier, A.L. Durier, C. Gauthier, R. Schirrer, Tribol. Int. 41 (2008) 975–984.
[21] J. Zhang, J. Zhang, Tribol. Lett. 49 (2013) 77–83.
[22] J. Schreiber, S. Vasnyov, J. Phys. Condens. Matter 16 (2004) S75–S84.
[23] R. Saha, W.D. Nix, Acta Mater. 50 (2002) 23–38.
[24] Y.R. Jeng, P.C. Tsai, Y.H. Liu, Mater. Res. Bull. 44 (2009) 1995–1999.
[25] K. Shinozaki, T. Honma, T. Komatsu, Mater. Res. Bull. 46 (2011) 922–928.